Journal of Magnetic Resonance 213 (2011) 76–81

Contents lists available at SciVerse ScienceDirect

Journal of Magnetic Resonance

journal homepage: www.elsevier.com/locate/jmr

Radiation damping on cryoprobes

Dmitry Shishmarev, Gottfried Otting *

Research School of Chemistry, Australian National University, Canberra, ACT 0200, Australia

ARTICLE INFO

Article history:
Received 8 July 2011
Revised 1 August 2011
Available online 10 September 2011

Keywords:
Radiation damping
Cryoprobe
NOESY
TOCSY
Water flip-back

ABSTRACT

Radiation damping on 600 and 800 MHz cryoprobes was investigated. The phase angle β between a vector 90° phase shifted to the precessing magnetization and the rf field induced in the coil was found to depend markedly on whether an FID was being acquired or not. The magnitude of the radiation damping field was sufficiently strong to restore 95% of the equilibrium water magnetization of a 90% H_2O sample in a 5 mm sample tube within about 5 ms following a 165° pulse. This can be exploited in water flip-back versions of NOESY and TOCSY experiments of proteins, but care must be taken to limit the effect of the radiation damping field from the water on the H^{α} protons. Long water-selective pulses can be applied only following corrections. We developed a program for correcting pulse shapes if β is non-zero. The WATERGATE scheme is shown to be insensitive to imperfections introduced by radiation damping.

1. Introduction

Radiation damping is associated with very intense NMR signals, e.g. the ^{1}H NMR resonance of water in an aqueous solution. By coupling the magnetization with the circuit of the radio-frequency (rf) coil, radiation damping returns transverse magnetization back to equilibrium much faster than T_1 relaxation processes. The phenomenon is well understood [1–4] and many ingenious ways have been designed to suppress radiation damping effects, including active feedback circuits [5–7], pulse shape compensation [8], bipolar gradients [9–11], trim pulses [12] and *Q*-switches [13]. The effect has also been exploited to achieve selective water flip-back, e.g. during the mixing times of NOESY and ROESY experiments [14,15], and for selective water excitation [16–18]. Controlling radiation damping is important, because it can perturb resonances with similar frequencies [16,18–21].

Radiation damping increases with the quality factor of the rf coil and therefore is particularly strong with cryogenic probes which achieve improved sensitivity by an increased quality factor compared with room temperature probes. To understand the peculiar appearance of FIDs measured for samples of 90% H_2O/10% D_2O on different cryoprobes, we determined the radiation damping parameters from indirectly and directly detected signals. While data were obtained using Bruker TCI cryoprobes, the effects from strong radiation damping apply to any probe with very high quality factor. The results show that different parameters apply during signal acquisition compared with free precession delays, that a strong water signal overloads the cold preamplifier and that radiation damping is sufficiently strong to be used for water flip-back in improved NOESY and TOCSY experiments.

2. Theory

Radiation damping of a single NMR signal can be described by [22]:

$$\omega_{+}^{RD}(t) = -i\alpha M_{+}(t)e^{-i\beta}\cos(\beta). \quad (1)$$

where $\omega_{+}^{RD}(t) = \omega_{x}^{RD}(t) + i\omega_{y}^{RD}(t)$ and $M_{+}(t) = M_x(t) + iM_y(t)$ are the complex forms of the radiation damping field and the transverse magnetization, respectively, α is the coefficient of proportionality between the transverse magnetization and the resulting radiation damping field and β is the phase angle between a vector orthogonal to the precessing magnetization and the rf field induced in the coil. When the probe is tuned exactly at electrical resonance, the RD field is at perfect quadrature with the transverse magnetization, i.e. $\beta = 0$. Since probe tuning usually minimizes reflected power rather than putting the probe at exact electrical resonance [23], β can be non-zero.

In the case of several resonances subject to radiation damping, the modified Bloch equations take the following form [22]:

* Corresponding author. Fax: +61 2 61250750.
E-mail address: gottfried.otting@anu.edu.au (G. Otting).

1090-7807/$ - see front matter © 2011 Elsevier Inc. All rights reserved.
doi:10.1016/j.jmr.2011.08.040

$$\frac{M_i^x(t)}{dt} = -\omega_i M_i^y(t) - R_2^i M_i^x(t) - \alpha\cos^2(\beta) M_i^z(t) \times \sum_j^N M_j^x(t) - \alpha\cos(\beta)\sin(\beta) M_i^z(t) \sum_j^N M_j^y(t);$$

$$\frac{M_i^y(t)}{dt} = \omega_i M_i^x(t) - R_2^i M_i^y(t) - \alpha\cos^2(\beta) M_i^z(t) \sum_j^N M_j^y(t) + \alpha\cos(\beta)\sin(\beta) M_i^z(t) \sum_j^N M_j^x(t);$$

$$\frac{M_i^z(t)}{dt} = R_1^i\left(M_0^i - M_i^z(t)\right) + \alpha\cos(\beta)\left(\cos(\beta) M_i^x(t) - \sin(\beta) M_i^y(t)\right) \sum_j^N M_j^x(t) + \alpha\cos(\beta)\left(\cos(\beta) M_i^y(t) + \sin(\beta) M_i^x(t)\right) \sum_j^N M_j^y(t) \quad (2)$$

where R_1 and R_2 are the longitudinal and transverse relaxation rates and the indices i and j identify resonances at different frequencies. In these equations, α is in units of rad/s. In the following, we specify this radiation damping parameter in Hz, i.e. $\alpha_{Hz} = \alpha/2\pi$.

3. Results

3.1. Measurement of the radiation damping parameters α and β

3.1.1. RD parameters of a FID – isopropanol

The radiation damping parameters α and β prevailing during acquisition of an FID can be estimated from the appearance of the 1D NMR spectrum of a sample of 90% isopropanol/10% DMSO-d_6 measured after a small flip-angle excitation pulse. The RD fields from each of the two doublet components of the methyl resonance mutually affect their time evolution in a manner that yields a symmetrical methyl resonance only when $\beta = 0$ [22].

Fig. 1 shows that the intense RD field of a cryoprobe severely affects the appearance not only of the doublet of the isopropanol methyl resonance but also of its ^{13}C satellites. The lineshapes could readily be simulated with a Python script (provided in the Supporting Information) using Eq. (2) for six resonances (two doublet components and four satellite lines). A 10° change in β significantly changes the appearance and symmetry of the doublet. Following tuning of the probe as recommended by the manufacturer (using the Bruker "wobb" command) to produce a maximal Q factor on resonance (599.991 MHz), the RD parameters were determined to be $\alpha_{Hz} = 35$ Hz and $\beta = 44°$. Repeating the experiment on a 800 MHz Bruker Avance NMR spectrometer equipped with the same type of cryoprobe (manufactured in 2005) yielded $\alpha_{Hz} = 32$ Hz and $\beta = 30°$ when tuned to the Larmor frequency (800.126 MHz). This means that neither probe is at exact electrical resonance following tuning to the ^1H Larmor frequencies. Nonetheless, measurements of signal-to-noise performed with a standard ethylbenzene sample at different tuning frequencies confirmed that tuning to the exact Larmor frequency produced the maximal sensitivity (data not shown).

3.1.2. RD parameters of a FID – water

To determine the sample dependence of the α and β parameters, we also measured the time domain signals of water ^1H magnetization after an inversion pulse for a range of H_2O/D_2O samples containing between 90% and 10% H_2O. Following calculation of the magnitude values of the FIDs, it is particularly easy to visualize the increase and decrease of transverse magnetization as radiation damping rotates the magnetization back to equilibrium.

Fig. 2 shows such magnitude FIDs for three samples containing 90%, 30% and 10% of H_2O on the 800 MHz spectrometer. Notably, the maximal signal observed for the 90% H_2O sample was not nine times greater than the maximal signal observed for the 10% H_2O sample. In addition, the FID of the 90% H_2O sample displayed a flat top that could not be reproduced in simulations using Eq. (2), whereas the FID of the 10% H_2O sample could readily be simulated. The result did not change when we placed an attenuator in the acquisition signal path. We believe that the cold preamplifier of the cryoprobe no longer operates in a linear regime when challenged by a large H_2O signal.

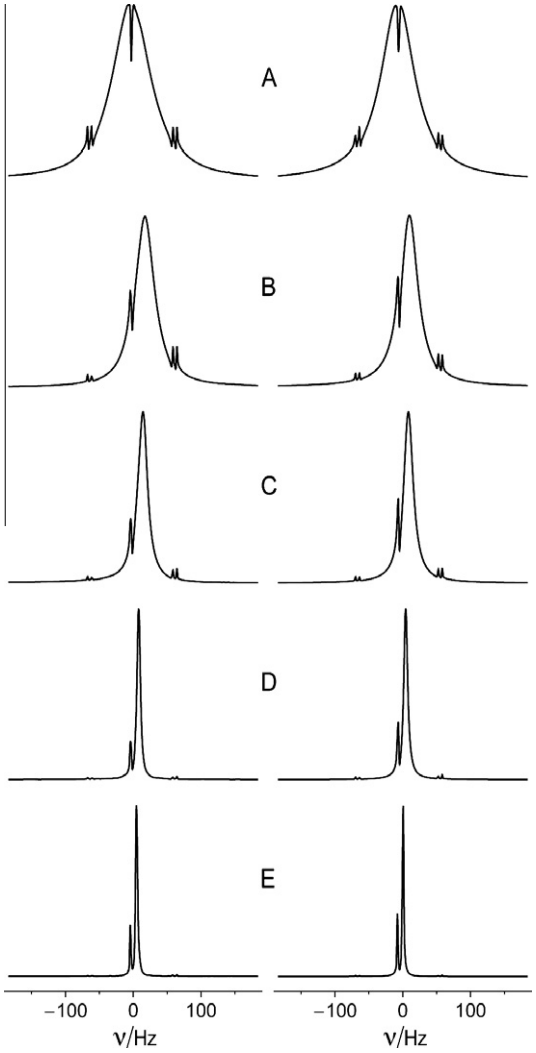

Fig. 1. Experimental 600 MHz ^1H NMR spectra of the isopropanol methyl doublet including its ^{13}C satellites of a 90%/10% v/v mixture of isopropanol/DMSO-d_6 in a 5 mm sample tube recorded after a 9° excitation pulse at different tuning frequencies (TF). The data were recorded on a Bruker Avance 600 NMR spectrometer equipped with a triple-resonance $^1H/^{13}C/^{15}N$ TCI cryoprobe with single-axis gradient coil (built in 2007). The left and right panels display the experimental and simulated spectra, respectively. The simulated spectra were calculated using $\alpha_{Hz} = 35$ Hz throughout, whereas the phase angles β were adjusted for a best fit between the simulated and experimental data. $T_1 = 7$ s and $T_2 = 5$ s as in Barjat et al. [22]. The spectra were scaled to the same height of the maximum point. (A) TF = 599.345 MHz, $\beta = 3°$; (B) TF = 599.991 MHz, $\beta = 44°$; (C) TF = 600.448 MHz, $\beta = 58°$; (D) TF = 601.686 MHz, $\beta = 71°$; (E) TF = 602.552 MHz, $\beta = 81°$.

The best fit of the FID obtained with the 10% H_2O sample using Eq. (2) gave $\alpha_{Hz} = 25.4 \pm 0.6$ Hz and $\beta = 35.0 \pm 1.1°$. This shows that the β angle is only to a small degree sample dependent. For the samples with higher H_2O content, the strength of the RD field can be estimated by the width of the trace (the time τ_{rec}) at a height, where the cold preamplifier would not be overloaded (Fig. 2). As a consequence of a non-zero β parameter, the magnetization changes its phase in a non-linear manner during its return to the z-axis.

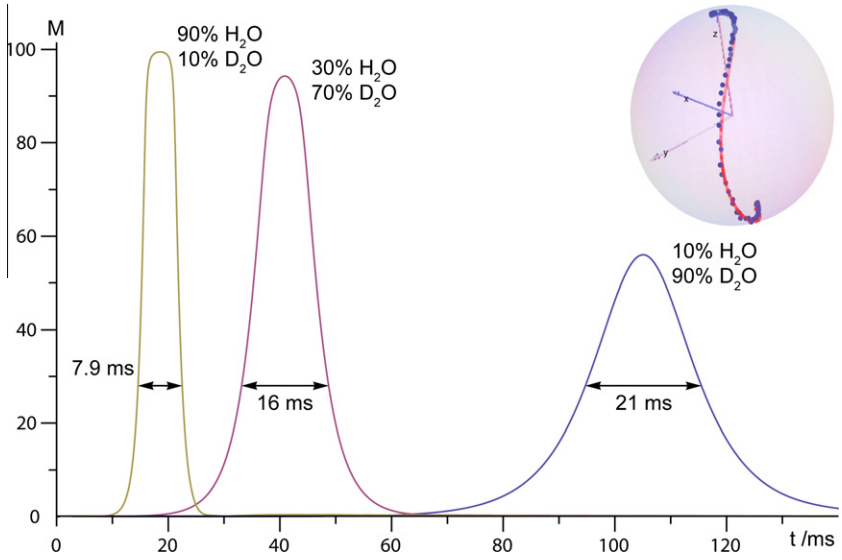

Fig. 2. Experimental FIDs recorded on a 800 MHz Bruker Avance NMR spectrometer equipped with a triple-resonance $^{1}H/^{13}C/^{15}N$ cryoprobe with single-axis gradient coil after an inversion pulse followed by a 40 G/cm pulsed field gradient of 0.9 ms duration for samples with different v/v ratios of H_2O to D_2O. Magnitude values are displayed. The vertical axis measures the detected magnetization in arbitrary units. The insert compares the experimental and simulated trajectory of the 10% H_2O sample, showing the trace described on the surface of a sphere by the endpoint of the magnetization vector as it rotates back to the *z*-axis due to the RD field. R_1 and R_2 relaxation rates were neglected and the *z*-component of the magnetization was calculated from the measured *x*- and *y*-components to generate a vector of unit length. Note the pronounced change in phase throughout the magnetization trajectory due to the non-zero β value.

3.1.3. RD parameters during free precession delays

As direct detection of FIDs of samples with more than 10% H_2O gave unreliable results, we also determined the RD parameters of water samples indirectly. For reproducible phase-sensitive results, the magnetization trajectories were monitored following a 165° excitation pulse. Three different pulse sequences were used to measure signals proportional to the *x*, *y* and *z* components of the magnetization by a small readout pulse (Fig. 3A and B).

Fig. 3C and D shows the magnetization trajectories measured indirectly for the 90% H_2O/10% D_2O sample on our 600 MHz and 800 MHz NMR spectrometers. The carrier frequency was set at the water resonance. Best fits using Eq. (2) yielded β angles of 10.7° and 2.4° for the two different spectrometers, i.e. values significantly smaller than in the direct detection experiments.

Table 1 summarizes the RD parameters measured directly and indirectly on the 800 MHz NMR spectrometer. The data of the 10% H_2O/90% D_2O sample indicated that the value of the α_{Hz} parameter was the same in the direct and indirect detection mode. Furthermore, using the indirectly measured α_{Hz} value and the β angle determined by direct measurement with the 10% H_2O/90% D_2O sample reproduced the τ_{rec} intervals observed in the magnitude FIDs of Fig. 2, suggesting that α does not change when the cold preamplifier is overloaded and that the direct and indirect detection modes differ only in the β angle (Table 2). This difference can be

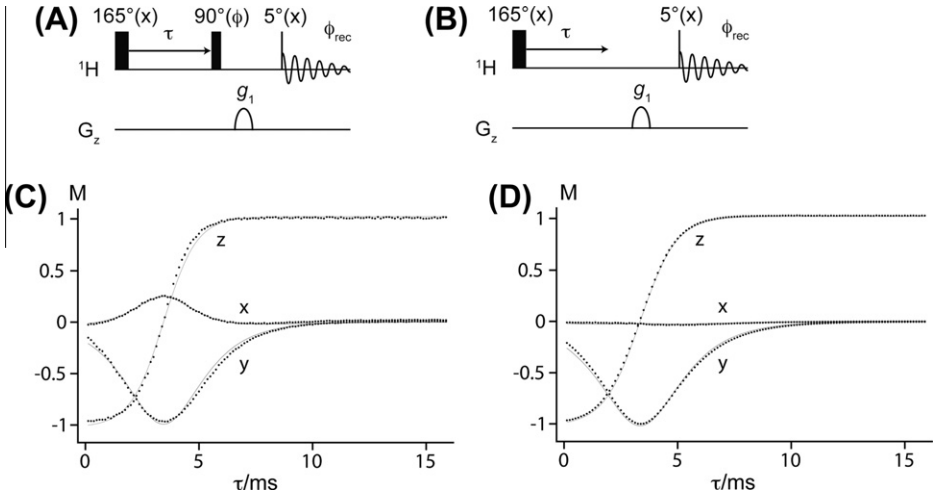

Fig. 3. RD-driven recovery of magnetization of a 90% H_2O/10% D_2O sample following a 165° pulse. (A) Pulse sequence used for the indirect measurement of the *x*- and *y*-component of the water magnetization. Phase cycle for measurement of the *x*-component: $\phi = y, -y$; receiver = $x, -x$. The gradient is sine-shaped (0.9 ms, 40 G/cm), followed by a recovery delay of 0.2 ms. The carrier frequency is at the water resonance. The amplitude of the FID was recorded in 128 experiments, where the delay τ was incremented in steps of 125 μs. Detection of the *y*-component used the same parameters, except that $\phi = x, -x$. (B) Detection of the *z*-component. (C) Experimental results obtained at 600 MHz with the pulse sequences in (A) and (B). The vertical axis measures the fraction of total magnetization. The best fits (solid lines) were simulated using the Mathematica [26] script provided in the Supporting Information. The fitted RD parameters are: $\alpha_{Hz} = 110.5 \pm 1.4$ Hz, $\beta = 10.7 \pm 0.9°$. (D) Same as (C), but at 800 MHz. The fitted RD parameters are: $\alpha_{Hz} = 98.6 \pm 0.5$ Hz, $\beta = 2.4 \pm 0.8°$.

Table 1
RD parameters measured by direct and indirect detection.[a]

RD parameters	Indirect measurement		Direct measurement	
	α_{Hz} (Hz)	β (°)	α_{Hz} (Hz)	β (°)
90% H_2O/10% D_2O	98.6 ± 0.5	2.4 ± 0.8	–	–
30% H_2O/70% D_2O	39.0 ± 0.3	−1.0 ± 0.6	–	–
10% H_2O/90% D_2O	25.2 ± 0.5	0.4 ± 0.5	25.4 ± 0.6	35.0 ± 1.1

[a] Data recorded on a 800 MHz NMR spectrometer with triple-resonance cryoprobe using 5 mm sample tubes.

Table 2
τ_{rec} intervals obtained by direct and indirect detection.[a]

	τ_{rec}/ms (measured indirectly) [b]	τ_{rec}/ms (measured directly) [c]	τ_{rec}/ms (calculated) [d]
90% H_2O/10% D_2O	5.2	7.9	7.8
30% H_2O/70% D_2O	13	16	16
10% H_2O/90% D_2O	16	21	21

[a] τ_{rec} was defined by reference to 50% of the total ^1H magnetization in the 10% H_2O/90% D_2O sample, $M_{50\%}$. In a magnitude FID monitoring the magnetization trajectory following an inversion pulse, τ_{rec} is the time between the first and second

attributed to the different rf pathways used in the cryoprobes during pulsing and detection, where only the direct detection pathway includes the cold preamplifier, altering the tuning characteristics of the rf circuit.

3.2. Applications

3.2.1. WATERGATE

The intense RD field associated with cryoprobes leads to a very rapid return of transverse water magnetization back to equilibrium, restoring >95% of the equilibrium magnetization in less than 5 ms (Fig. 3C and D). Consequently, the RD field seriously affects the effective shapes of even fairly short water-selective pulses.

Fig. 4 shows simulated results for the WATERGATE pulse sequence [24]. In the absence of radiation damping, the *z*-magnetization of the water is turned into transverse magnetization by the first selective 90° pulse and returned to the *z*-axis by the second selective 90° pulse (Fig. 4A). In the presence of radiation damping, the water magnetization remains to a large extent along the *z*-axis after the first selective pulse, is turned into negative magnetization by the 180° pulse and returns to the positive *z*-axis only with assistance by the RD field (Fig. 4B). Fortuitously, however, the final result is almost the same as in the absence of radiation damping.

It has been shown for conventional NMR probes and in the case of $\beta = 0$, that the pulse shapes can readily be corrected if α is known [8,25]. We followed the same strategy to correct the pulse shape if both radiation damping parameters α and β are non-zero. (A Mathematica [26] script is provided in the Supporting Information.) This correction allowed selective excitation of the water signal with pulses as long as 20 ms and we used it to generate 5 ms water-selective sinc 90° pulses. Next we used this corrected selective pulse in the experiment $90°(sel.)_x - 90°(non\text{-}sel.)_{-x}$ followed by the WATERGATE pulse sequence. In agreement with the simulations of Fig. 4, using the WATERGATE pulse element with or without RD-compensated selective pulse had no noticeable influence on the appearance of protein NMR spectra.

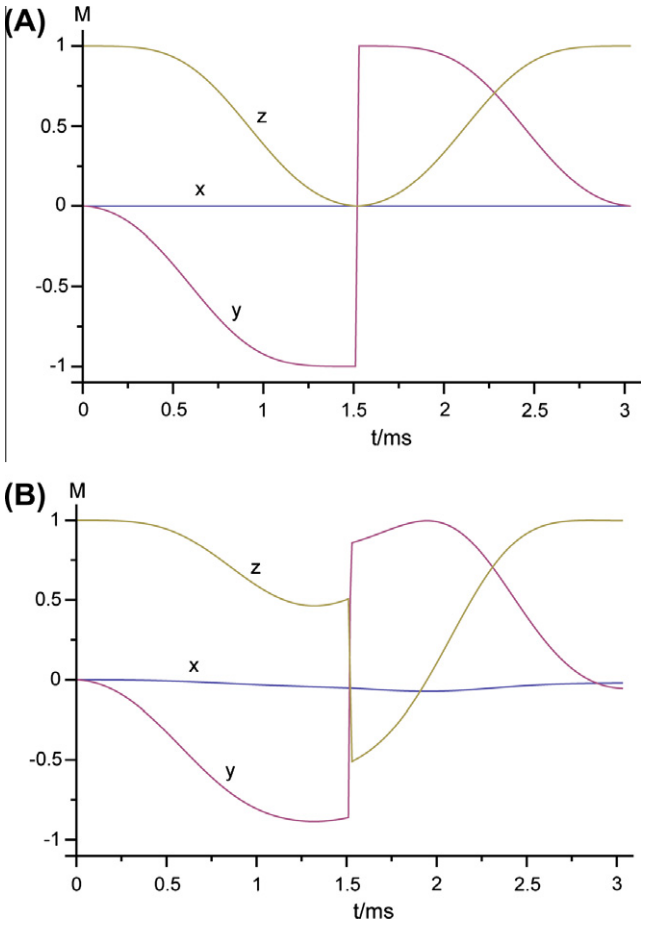

Fig. 4. Simulation of magnetization trajectories during the central element of a WATERGATE pulse sequence consisting of a 1.5 ms sinc-shaped water-selective pulse, a 20 μs 180° pulse and another 1.5 ms sinc pulse, starting from *z*-magnetization. (A) Without radiation damping. (B) With radiation damping with the parameters $\alpha_{Hz} = 110.5$ Hz and $\beta = 10.7°$.

3.2.2. RD-driven water flip-back

The extraordinarily fast recovery of equilibrium magnetization can be exploited in water flip-back versions of NOESY and TOCSY experiments by inserting a short delay τ_{RD} for RD-driven water flip-back at the end of the mixing period. During this delay, the water magnetization returns to the positive *z*-axis regardless of its previous orientation. Any remaining transverse component is dephased by a pulsed field gradient (g_4 in Fig. 5). A subsequent RD-compensated water-selective 90° pulse followed by a non-selective 90° pulse of opposite phase and the WATERGATE sequence excites the protein magnetization while maintaining water flip-back conditions. Prior to the flip-back delay, radiation damping is suppressed by bipolar gradients [9,27].

The duration of the delay τ_{RD} can be minimized by avoiding complete inversion of the water magnetization at the start of the delay. This is readily achieved by placing the carrier frequency on the water resonance and applying a phase shift of 45° between the two 90° pulses surrounding the evolution time t_1 [28].

It turns out that, on cryoprobes, it is important to allow the RD-driven water flip-back only towards the end of the mixing time rather than at the start of the mixing time. Fig. 6 compares the results of 2D NMR spectra recorded with the pulse sequences of Fig. 5. When radiation damping is allowed to act on the water magnetization already from the start of the mixing time, not only the water-protein cross-peaks are strongly attenuated but also the cross-peaks of H^{α} resonances near the water chemical shift (Fig. 6A). Allowing RD-driven water flip-back only towards the

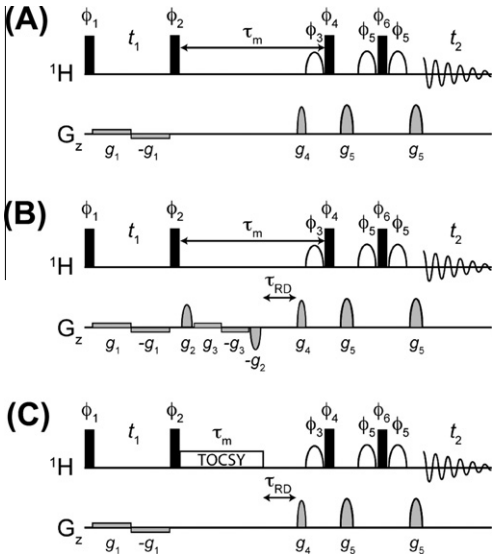

Fig. 5. 2D NOESY and TOCSY pulse sequences with water flip-back. Narrow and wide bars represent 90° and 180° pulses, respectively. The H_2O-selective 90° flip-back pulse at the end of the mixing time is a 5 ms RD-compensated sinc pulse, using only the center lobe of the sinc shape. The two H_2O-selective WATERGATE pulses are 1.5 ms 90° sinc pulses. The transmitter frequency is at the water resonance. The duration of the bipolar g_1 gradient pair is incremented along with the evolution time t_1. The gradients g_2, g_4 and g_5 were sine-shaped and of 0.9 ms duration. Gradients g_4 and g_5 were followed by a 0.2 ms recovery delay. Gradient strengths: g_1 = 1 G/cm; g_2 = 20 G/cm; g_3 = 1 G/cm; g_4 = 25 G/cm; g_5 = 30 G/cm. Phase cycle: $\phi_1 = (x, -x)$; $\phi_2 = 4(x + 45°, -x + 45°)$; $\phi_3 = 2(-x), 2(x)$; $\phi_4 = 2(x), 2(-x)$; $\phi_5 = (y)$; $\phi_6 = (-y)$; $\phi_{rec} = (x, -x, -x, x, -x, x, x, -x)$. τ_{RD} = 10 ms. (A) NOESY pulse sequence with RD-driven water flip-back starting at the start of the mixing time τ_m. (B) Improved NOESY pulse sequence, where RD-driven water flip-back occurs only at the end of the mixing time during the delay τ_{RD}. The bipolar gradients g_3 are applied for most of the mixing time τ_m to suppress radiation damping. (C) TOCSY pulse sequence with RD-driven water flip-back at the end of the mixing time.

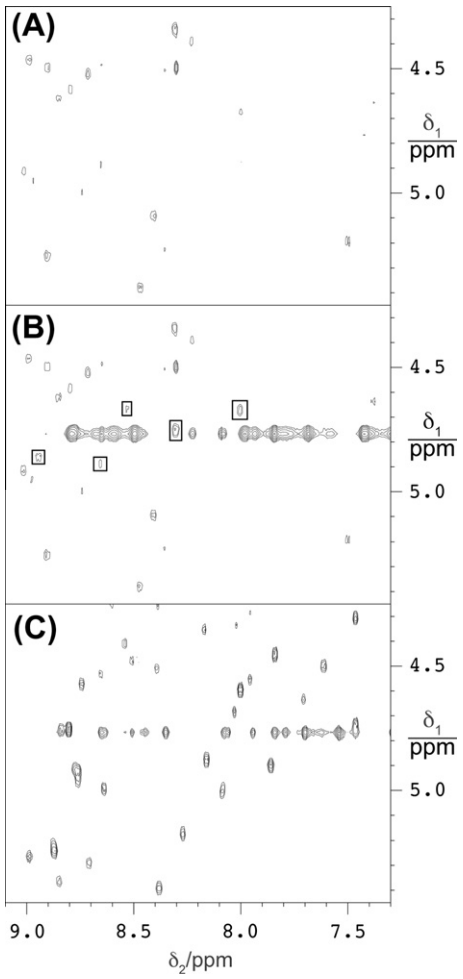

Fig. 6. Protein NOESY and TOCSY spectra recorded with the pulse sequences of Fig. 5. Only the spectral region containing H^{α}–H^{N} cross-peaks is shown. The sample was a 0.5 mM solution of ubiquitin fused to a 15-residue peptide in 90% H_2O/10% D_2O at pH 7.0 and 25 °C. The spectra were recorded on a Bruker Avance 800 MHz NMR spectrometer equipped with a triple-resonance TCI cryoprobe. The recovery delay between scans was 1 s. (A) NOESY spectrum recorded with the pulse sequence of Fig. 5A. τ_m = 60 ms. (B) Same as A, except using the pulse sequence of Fig. 5B. The same contour levels are plotted as in A. The lowest contour level was deliberately chosen high above the level of white noise to facilitate comparison of the cross-peak intensities. The band of intense peaks in the middle of the spectrum is produced by water-protein cross-peaks. (C) TOCSY spectrum recorded with the pulse sequence of Fig. 4C. The clean CITY [35] sequence was used for 60 ms of TOCSY mixing at a field-strength of 10 kHz.

end of the mixing time restores the water-protein cross-peaks and the cross-peaks nearby (Fig. 6B and C). Suppression of radiation damping during the earlier part of the experiment is achieved by the use of bipolar gradients during the evolution time t_1 [9] and during the mixing time (Fig. 5B). During TOCSY mixing, the spin-locking effect of the mixing sequence already achieves RD suppression (Fig. 5C [3]) which can be assisted by a weak gradient if necessary [29]. On our spectrometers, a RD-driven flip-back delay of 10 ms was sufficient to ensure facile water suppression by the following WATERGATE sequence, whereas a delay of 5 ms proved to be too short.

4. Discussion

The present work shows that, as the paths of pulse rf and detected rf are different in probeheads containing a cold preamplifier, also the radiation damping parameters can be different between directly and indirectly observed magnetization trajectories. In our cryoprobes, a non-zero β angle is sustained during acquisition, resulting in a slower return of the solvent magnetization to its equilibrium position and, hence, a narrower solvent signal (Fig. 1). Therefore, inspection of the FID observed after an inversion pulse easily leads one to underestimate the actual RD-field strength acting during a pulse sequence, especially if the most intense part of the signal is attenuated by preamplifier overload. Using a sample of concentrated isopropanol, non-zero β angles are easily detected.

The strong radiation damping field associated with cryoprobes makes it harder to control intense solvent signals but also opens new opportunities for convenient water flip-back. Water flip-back is essential for maximal sensitivity in biomolecular NMR experiments in water [30]. For proton probeheads operating at room temperature, α_{Hz} values in the range of 15–30 Hz have been reported [17,31]. (In the literature, the inverse of the RD parameter α is often quoted as the RD constant τ_r in seconds, where $\tau_r = 1/\alpha$. To avoid confusion with angular frequencies, we refer exclusively to α_{Hz} in Hz.) On a cryoprobe, α_{Hz} can be as large as 160 Hz [32]. The α_{Hz} values on our 600 and 800 MHz NMR spectrometers are about 110 and 100 Hz, respectively, for a 5 mm sample tube containing 90% H_2O. These radiation-damping constants are sufficient for RD-driven water flip-back delays τ_{RD} as short as 10 ms. Considering that the action of the RD field can be represented as a soft flip-back pulse applied at the frequency of the resonance interacting with the rf coil, it is clear that such strong RD fields can have detrimental effects on solute resonances nearby.

RD-driven water flip-back delays have been proposed previously, but their use with conventional probe-heads lead to the recommendation to use the entire NOESY mixing time to achieve the flip-back [14,33]. As shown in Fig. 6, cryoprobes require a modified

strategy, as a rapid, complete water-flip back early in the mixing time suppresses not only water-protein cross-peaks but also the cross-peaks of solute signals nearby. Allowing for RD-driven water flip-back at the end of the mixing time restores the cross-peaks and presents a strategy that can also readily be applied to TOCSY experiments and, by straightforward extension, to ROESY and 3D NOESY-HSQC and TOCSY-HSQC experiments.

On cryoprobes, achieving water flip-back by a short delay yields far more robust water suppression than active manipulation of the water magnetization by a series of phase-cycled water-selective 90° pulses [27,34] as each selective pulse would have to be compensated separately for radiation damping effects. Since these compensations depend on the magnitude of steady-state magnetization, the pulses would easily be miscalibrated. We expect that RD-driven water flip-back delays at the end of NOESY and TOCSY mixing times will become a routinely used feature of multidimensional NMR experiments performed in aqueous solution on cryogenic probeheads.

Acknowledgments

The authors thank Dr. Hiromasa Yagi for the sample of the ubiquitin construct and Professors Steffen Glaser and Malcolm Levitt for helpful discussions. G.O. thanks the Alexander von Humboldt Foundation for a Research Award that allowed initial measurements at the Technical University of Munich (Germany). Financial support by the Australian Research Council is gratefully acknowledged.

Appendix A. Supplementary material

Supplementary data associated with this article can be found, in the online version, at doi:10.1016/j.jmr.2011.08.040.

References

[1] N. Bloembergen, R.V. Pound, Radiation damping in magnetic resonance experiments, Phys. Rev. 95 (1954) 8–12.
[2] S. Bloom, Effects of radiation damping on spin dynamics, J. Appl. Phys. 28 (1957) 800–805.
[3] W.S. Warren, S.L. Hammes, J.L. Bates, Dynamics of radiation damping in nuclear magnetic resonance, J. Chem. Phys. 91 (1989) 5895–5904.
[4] M.P. Augustine, Transient properties of radiation damping, Prog. NMR Spectrosc. 40 (2002) 111–150.
[5] P. Broekaert, J. Jeener, Suppression of radiation damping in NMR in liquids by active electronic feedback, J. Magn. Reson. A 113 (1995) 60–64.
[6] A. Louis-Joseph, D. Abergel, J. Lallemand, Neutralization of radiation damping by selective feedback on a 400 MHz spectrometer, J. Biomol. NMR 5 (1995) 212–216.
[7] D.I. Hoult, G. Kolansky, D. Kripiakevich, A 'Hi-fi' Cartesian feedback spectrometer for precise quantitation and superior performance, J. Magn. Reson. 171 (2004) 57–63.
[8] J.-H. Chen, A. Jerschow, G. Bodenhausen, Compensation of radiation damping during selective pulses in NMR spectroscopy, Chem. Phys. Lett. 308 (1999) 397–402.
[9] V. Sklenář, Suppression of radiation damping in multidimensional NMR experiments using magnetic field gradients, J. Magn. Reson. A 114 (1995) 132–135.
[10] A. Böckmann, E. Guittet, Suppression of radiation damping during selective excitation of the water signal: the WANTED sequence, J. Biomol. NMR 8 (1996) 87–92.
[11] P.S.C. Wu, G. Otting, SWET for secure water suppression on probes with high quality factor, J. Biomol. NMR 32 (2005) 243–250.
[12] G. Otting, Improved resolution and sensitivity in NOE and ROE experiments with water by the use of B_1 gradients, J. Magn. Reson. B 103 (1993) 288–291.
[13] C. Anklin, M. Rindlisbacher, G. Otting, F.H. Laukien, A probehead with switchable quality factor. Suppression of radiation damping, J. Magn. Reson. B 106 (1995) 199–201.
[14] G. Lippens, C. Dhalluin, J.-M. Wieruszeski, Use of a water flip-back pulse in the homonuclear NOESY experiment, J. Biomol. NMR 5 (1995) 327–331.
[15] D.B. Fulton, F. Ni, ROESY with water flip back for high-field NMR of biomolecules, J. Magn. Reson. 129 (1997) 93–97.
[16] G. Otting, E. Liepinsh, Selective excitation of intense solvent signals in the presence of radiation damping, J. Biomol. NMR 5 (1995) 420–426.
[17] A.G. Sobol, G. Wider, H. Iwai, K. Wüthrich, Solvent magnetization artifacts in high-field NMR studies of macromolecular hydration, J. Magn. Reson. 130 (1998) 262–271.
[18] G. Wider, R. Riek, K. Wüthrich, Diffusion filters for separation of solvent-protein and protein–protein nuclear overhauser effects (HYDRA), J. Am. Chem. Soc. 118 (1996) 11629–11634.
[19] R. Freeman, W.A. Anderson, Nuclear magnetic double resonance. Transmission of modulation information through the nuclear spin–spin coupling, J. Chem. Phys. 42 (1965) 1199–1229.
[20] M. Guéron, P. Plateau, M. Decorps, Solvent signal suppression in NMR, Prog. NMR Spectrosc. 23 (1991) 135–209.
[21] J. Jeener, A. Vlassenbroek, P. Broekaert, Unified derivation of the dipolar field and relaxation terms in the Bloch–Redfield equations of liquid NMR, J. Chem. Phys. 103 (1995) 1309–1332.
[22] H. Barjat, G.P. Chadwick, G.A. Morris, A.G. Swanson, The behavior of multiplet signals under "radiation damping" conditions. I. Classical effects, J. Magn. Reson. A 117 (1995) 109–112.
[23] D. Marion, H. Desvaux, An alternative tuning approach to enhance NMR signals, J. Magn. Reson. 193 (2008) 153–157.
[24] M. Piotto, V. Saudek, V. Sklenář, Gradient-tailored excitation for single-quantum NMR spectroscopy of aqueous solutions, J. Biomol. NMR 2 (1992) 661–665.
[25] B. Cutting, J.-H. Chen, D. Moskau, G. Bodenhausen, Radiation damping compensation of selective pulses in water-protein exchange spectroscopy, J. Biomol. NMR 17 (2000) 323–330.
[26] Wolfram Research, Inc., Mathematica, Version 8.0, Champaign, IL, 2010.
[27] D.B. Fulton, R. Hrabal, F. Ni, Gradient-enhanced TOCSY experiments with improved sensitivity and solvent suppression, J. Biomol. NMR 8 (1996) 213–218.
[28] W. Jahnke, M. Baur, G. Gemmecker, H. Kessler, Improved accuracy of NMR structures by a modified NOESY-HSQC experiment, J. Magn. Reson. B 106 (1995) 86–88.
[29] T.L. Hwang, S. Mori, A.J. Shaka, P.C.M. van Zijl, Application of phase-modulated CLEAN Chemical EXchange Spectroscopy (CLEANEX-PM) to detect water-protein proton exchange and intermolecular NOEs, J. Am. Chem. Soc. 119 (1997) 6203–6204.
[30] S. Grzesiek, A. Bax, The importance of not saturating H_2O in protein NMR – application to sensitivity enhancement and NOE measurements, J. Am. Chem. Soc. 115 (1993) 12593–12594.
[31] J.-H. Chen, B. Cutting, G. Bodenhausen, Measurement of radiation damping rate constants in nuclear magnetic resonance by inversion recovery and automated compensation of selective pulses, J. Chem. Phys. 112 (2000) 6511–6514.
[32] S.Y. Huang, C. Anklin, J.D. Walls, Y.Y. Lin, Sizable concentration-dependent frequency shifts in solution NMR using sensitive probes, J. Am. Chem. Soc. 126 (2004) 15936–15937.
[33] J.M. Gruschus, J.A. Ferretti, ^{15}N-edited three-dimensional NOESY-HMQC with water flipback: enhancement of weak labile ^{1}H resonances of protein side chains contacting DNA, J. Magn. Reson. 135 (1998) 87–92.
[34] C. Dhalluin, J.-M. Wieruszeski, G. Lippens, An improved homonuclear TOCSY experiment with minimal water saturation, J. Magn. Reson. B 111 (1996) 168–170.
[35] J. Briand, R.R. Ernst, Computer-optimized homonuclear TOCSY experiments with suppression of cross relaxation, Chem. Phys. Lett. 185 (1991) 276–285.